Gravity Field of the Moon from the Gravity Recovery and Interior Laboratory (GRAIL) Mission

Maria T. Zuber *et al.*

Science **339**, 668 (2013);
DOI: 10.1126/science.1231507

Gravity Field of the Moon from the Gravity Recovery and Interior Laboratory (GRAIL) Mission

Maria T. Zuber,[1*] David E. Smith,[1] Michael M. Watkins,[2] Sami W. Asmar,[2] Alexander S. Konopliv,[2] Frank G. Lemoine,[3] H. Jay Melosh,[4] Gregory A. Neumann,[3] Roger J. Phillips,[5] Sean C. Solomon,[6,7] Mark A. Wieczorek,[8] James G. Williams,[2] Sander J. Goossens,[9] Gerhard Kruizinga,[2] Erwan Mazarico,[1] Ryan S. Park,[2] Dah-Ning Yuan[2]

Spacecraft-to-spacecraft tracking observations from the Gravity Recovery and Interior Laboratory (GRAIL) have been used to construct a gravitational field of the Moon to spherical harmonic degree and order 420. The GRAIL field reveals features not previously resolved, including tectonic structures, volcanic landforms, basin rings, crater central peaks, and numerous simple craters. From degrees 80 through 300, over 98% of the gravitational signature is associated with topography, a result that reflects the preservation of crater relief in highly fractured crust. The remaining 2% represents fine details of subsurface structure not previously resolved. GRAIL elucidates the role of impact bombardment in homogenizing the distribution of shallow density anomalies on terrestrial planetary bodies.

The Moon is a key to deciphering the evolutionary history of the terrestrial planets because it is the most accessible planetary body that preserves a surface record spanning most of solar system history. Reconstructing the evolution of a planet requires an understanding of the structure of its interior, which contains information on bulk composition, differentiation, and the nature of heat generation and heat loss that has influenced the style, extent, and duration of volcanism and tectonics. The Gravity Recovery and Interior Laboratory (GRAIL) mission (*1*) was undertaken to map the lunar gravity field to address, in the context of other remote sensing and in situ observations, fundamental questions about lunar evolution.

Aside from the influence of the Moon's gravity throughout Earth history in producing oceanic tides, lunar gravity has been an observation of interest since the earliest satellites orbited the Moon and revealed the presence of mass concentrations or "mascons" associated with the large nearside impact basins (*2*). The Moon's synchronous rotation, which causes the same hemisphere to always face Earth, poses a special challenge in measuring gravity. The most common method entails measuring the frequency shift of a spacecraft's radio signal directly from a tracking station on Earth, but such a measurement cannot be made on the Moon's farside. One approach to measuring farside gravity is through the use of a relay satellite, as was done by the recent Kaguya mission (*3*). Current spherical harmonic (*4*) lunar gravity models derived from tracking Lunar Prospector (LP) and earlier orbiters (*5*–*7*) and from the more recent Kaguya orbiter (*3*) range from degree and order 100 to 150, providing an effective block size resolution of 54 to 36 km, respectively.

GRAIL is a spacecraft-to-spacecraft tracking mission at the Moon, developed with heritage from the Gravity Recovery and Climate Experiment (GRACE) mission (*8*) that is currently mapping Earth's gravity field and its temporal variability. Each GRAIL spacecraft has a single science instrument, the Lunar Gravity Ranging System (LGRS), which measures the change in distance between the two co-orbiting spacecraft as they fly above the lunar surface. The spacecraft are perturbed by the gravitational attraction of topography and subsurface mass variations that can be isolated and subsequently analyzed. Doing so requires correcting for perturbations due to spacecraft maneuvers, nonconservative forces such as solar radiation pressure and spacecraft outgassing, and relativistic effects (*4*).

GRAIL was launched successfully from Cape Canaveral Air Force Station on 10 September 2011, aboard a Delta-II 7290H. The twin spacecraft embarked on separate low-energy trajectories to the Moon via the EL-1 Lagrange point (*9*) and inserted into lunar polar orbit on 31 December 2011 and 1 January 2012. After a total of 27 maneuvers (*10*) to lower and circularize the orbits to ~55 km mean altitude (figs. S1 and S2) and to align the spacecraft to their ranging configuration, GRAIL executed its primary mapping mission (PM) from 1 March through 30 May 2012, transmitting to Earth 637 MB of science data corresponding to >99.99% of possible data that could be collected. During the PM, the inter-spacecraft distance varied between 82 and 218 km (fig. S3) to provide different sensitivities to the short- and longer-wavelength components of the gravity field. As exemplified in fig. S4, the root mean square (RMS) range-rate residuals from the LGRS Ka-band (32 GHz) ranging system during the PM were generally on the order of 0.02 to 0.05 μm s^{-1}, a factor of 2 to 5 better than the mission requirements.

These observations have been integrated into a spherical harmonic representation of the lunar gravitational field, which we denote model GL0420A. This model extends to degree and order 420, corresponding to a spatial block size of 13 km. Gravity field determination requires the application of numerous corrections (*4*), and emphasis in the production of this model has been on resolving short-wavelength structure.

The global free-air gravity field of the Moon is shown in Fig. 1A and the Bouguer gravity in Fig. 1B. The latter reveals the gravitational structure of the subsurface after subtraction of the expected contribution of surface topography from the free-air gravity. As with previous lunar gravity models, the GRAIL field shows the prominent mascons, the largest of which are associated with nearside basins, as well as the broad structure of the highlands. However, the much higher spatial resolution and greatly improved signal quality as compared with previous models combine to reveal distinctive gravitational signatures of many features not previously resolved, including impact basin rings, central peaks of complex craters, volcanic landforms, and smaller simple bowl-shaped craters.

Understanding the spectral content of the observations facilitates interpretation of the gravity maps (Fig. 2A). As with other planetary potential field representations, the RMS power of lunar gravity is greatest at low degrees (long wavelengths) and least at high degrees (short wavelengths). The empirical best-fit power law to the lunar gravity field is $2.5 \times 10^{-4}\ l^{-2}$, where l is the spherical harmonic degree. The degree at which the error spectrum intersects the power spectrum traditionally represents the spatial scale at which the gravitational coefficients (eqs. S1 and S2) are 100% in error. However, our best estimate of the error spectrum of model GL0420A does not intersect the model power through degree 420, which indicates that still higher-resolution fields may ultimately be derived from GRAIL's PM data set. It is notable that GL0420A fits late-stage PM data (19 to 29 May 2012) when the periapsis altitude was ~17 to 25 km, at 1 to 1.5 μm or 10 to 15 times the intrinsic quality of the Ka-band range-rate observations. The gravitational powers of the LP and Kaguya fields are comparable and

[1]Department of Earth, Atmospheric and Planetary Sciences, Massachusetts Institute of Technology, Cambridge, MA 02139-4307, USA. [2]Jet Propulsion Laboratory, Pasadena, CA 91109, USA. [3]Solar System Exploration Division, NASA Goddard Space Flight Center, Greenbelt, MD 20771, USA. [4]Department of Earth, Atmospheric and Planetary Sciences, Purdue University, West Lafayette, IN 47907, USA. [5]Southwest Research Institute, Boulder, CO 80302, USA. [6]Department of Terrestrial Magnetism, Carnegie Institution of Washington, Washington, DC 20015, USA. [7]Lamont-Doherty Earth Observatory, Columbia University, Palisades, NY 10964, USA. [8]Institut de Physique du Globe de Paris, Sorbonne Paris Cité, Université Paris Diderot, Case 7071, Lamarck A, 5, rue Thomas Mann, 75205 Paris Cedex 13, France. [9]University of Maryland, Baltimore County, Baltimore, MD 21250, USA.

*To whom correspondence should be addressed. E-mail: zuber@mit.edu

approximately match that of GRAIL to about degree 100 (block size 54 km), but the GRAIL errors at spatial scales associated with large to intermediate impact basins [degrees ≤ 60 (90 km)] are three to five orders of magnitude smaller than those of the LP and Kaguya fields.

Owing to its direct sampling of farside gravity, the Kaguya field displays a higher coherence than that of LP (Fig. 2B); the Kaguya correlation peaks at approximately degree 60 and falls off rapidly with increasing degree because of an inability to sense the full gravitational power of smaller-scale mass variations. The LP data exhibit overly low global coherence at all degrees despite the lower mapping altitude (40 to 100 km) than Kaguya (100 km), though a recent reanalysis of LP observations (*11*) that focused on improving resolution where direct tracking is available shows a

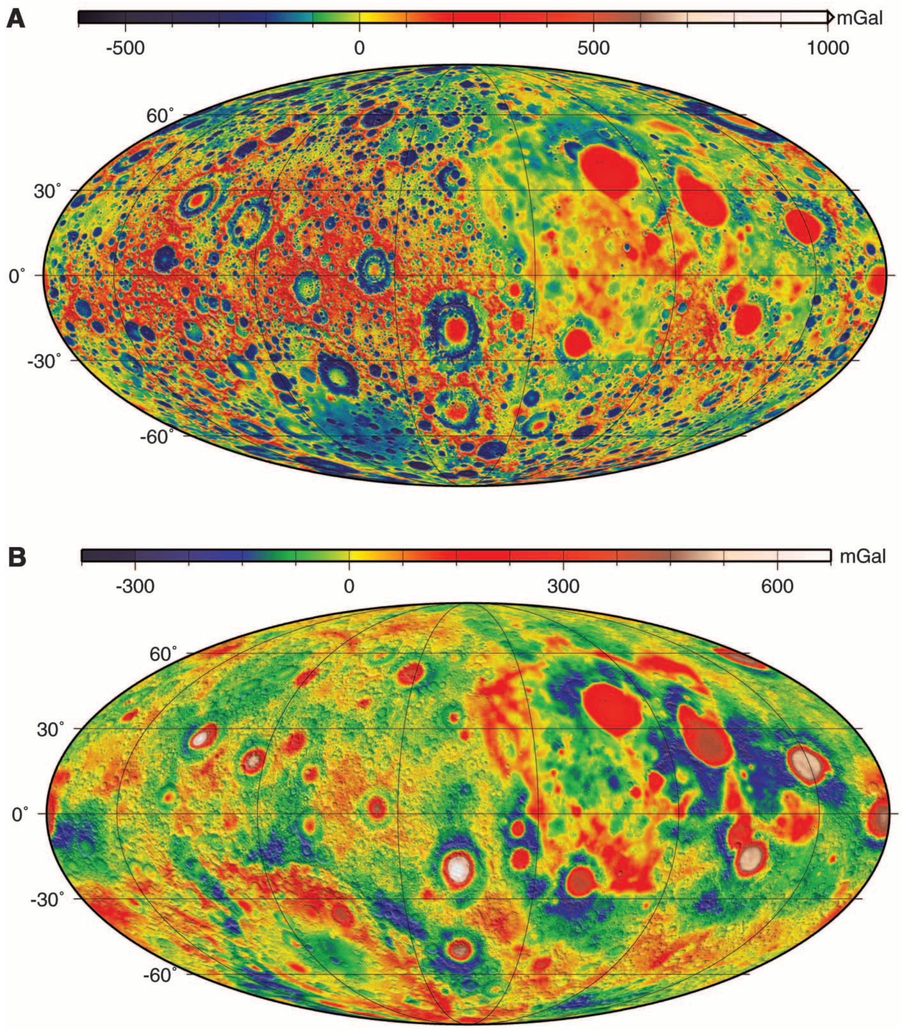

Fig. 1. (**A**) Free-air and (**B**) Bouguer gravity anomaly maps from GRAIL lunar gravity model GL0420A, to spherical harmonic degree and order 420. Maps are in Molleweide projection centered on 270°E longitude and show the nearside on the right and farside on the left. Gravity is plotted in units of milliGalileos, where 1000 mgal = 1 cm s^{-2}. A crustal density of 2560 kg m^{-3} was assumed in the Bouguer correction. For the Bouguer map, degrees <6 have been filtered out to highlight mid- to short-wavelength structure (*4*).

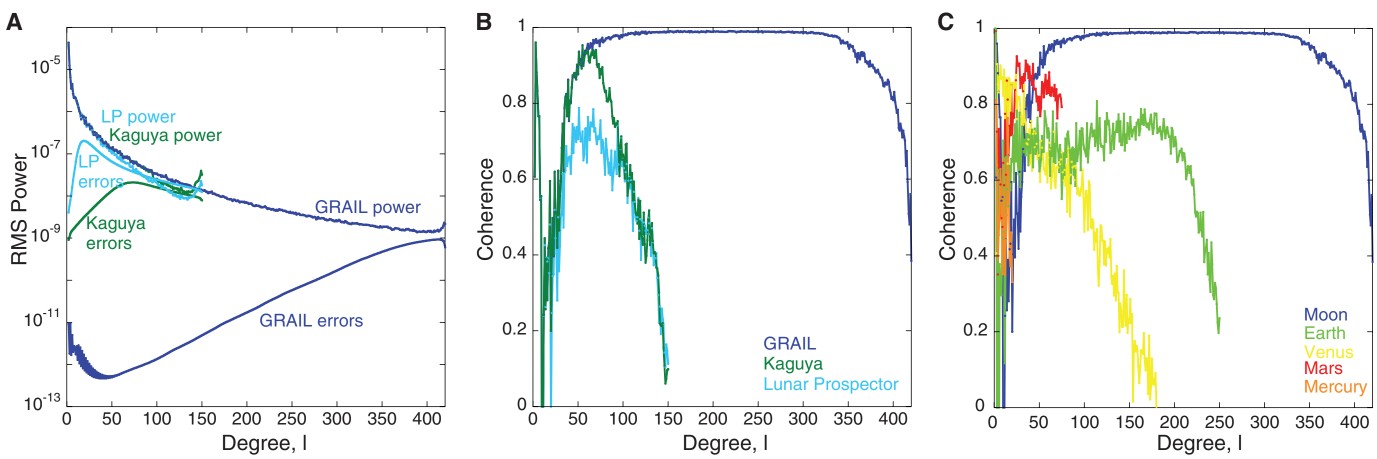

Fig. 2. (**A**) RMS power and (**B**) coherence versus harmonic degree for the gravity fields determined by GRAIL, Kaguya, and LP. (**C**) Comparison of coherence between gravity and topography versus degree for the Moon, with coherence for other terrestrial planets. In (B), all gravity models are compared with topography from the Lunar Orbiter Laser Altimeter (LOLA) (*23*). Data sets used in (C) are given in table S1.

higher nearside coherence. In contrast, GL0420A reveals a very high correlation with topography to high degrees. The departure of the coherence spectra of the LP and Kaguya fields from the GRAIL spectrum at degrees 30 and 60, respectively, indicates that despite approximately matching the power, these fields are significantly in error at higher degrees. Between degrees 80 (68 km) and 320 (17 km), 98.5% of the Moon's gravity signal is attributable to topography.

The magnitudes of short-wavelength Bouguer anomalies (Fig. 1B) are consistent with the high, but not perfect, coherence shown in Fig. 2B. Comparison of the maps shows that the range in Bouguer anomaly is typically up to ~10% that of the free-air gravity anomaly, which translates to a 1% ratio in terms of power. The lack of perfect correlation between gravity and topography is a result of lateral variations in subsurface density, such as those due to the presence of magmatic intrusions. Although this signal is small, the high-quality measurements ensure that it is easily resolvable (Fig. 2A) at a level that permits the investigation of processes associated with impact cratering, such as brecciation, ejecta deposition, impact melting, and magmatism.

In general, gravity and topography should become more highly correlated with increasing degree, because the strength of the lithosphere is increasingly able to support topographic loads at shorter wavelengths without compensating masses at depth, and because the signals associated with subsurface anomalies are increasingly attenuated at spacecraft altitude with increasing degree. The high coherence exhibited by the Moon (Fig. 2C) implies that the majority of the short-wavelength gravity signal is a result of surface topography, most of which is related to abundant impact craters. To retain a high coherence, the crust beneath those landforms must have been pervasively fractured and largely homogenized in density. Short-wavelength, lateral density variations due to magmatism, variable porosity, or regionally variable impact melting imparted during the early, post-accretional era of high impact flux are sparsely preserved at ~30- to 130-km scales. At harmonic degrees lower than about 60 (90 km), the coherence displays greater variability within the general pattern of a rapid decrease with decreasing degree. At these longer wavelengths, the lower coherence reflects the heterogeneity of lunar interior structure: thinning of the crust beneath impact basins, large-scale variations in crustal composition indicated by orbital remote sensing (*12*), and lateral variations in mantle composition and possibly temperature, such as the variations associated with the Procellarum KREEP Terrane (*13*, *14*). At the highest degrees (>330), the coherence falls off because of longitudinal gaps in the spacecraft ground tracks. As shown in Fig. 2C, the gravity-topography coherence exhibited by the Moon is unlike that observed for any other terrestrial planet. From degrees 25 to 200, Earth's coherence is variable, with an average value of ~0.7. The coherence spectrum reflects a contribution from the continents, whose gravity-topography relationships are dominated by crustal thickness variations and erosion, and include influences from compositional variability and tectonic and volcanic processes at shorter wavelengths. Earth's ocean basins also contribute to the correlation, and the interpretation of the combined contributions is complex. The coherence for Venus peaks at 0.9 at degree 3 and falls off rapidly at higher degrees. This falloff in coherence may reflect a combination of large-scale volcanic resurfacing (*15*) that smoothed the surface at short and intermediate length scales; the thick atmosphere, which screened small impacts; density anomalies related to mantle convection; and the orbital altitude of the Magellan spacecraft. The coherence for Mars is greatest at low degrees, at which it is governed by large-scale topography (*16*) such as the Tharsis province (*17*). Mercury's coherence does not exceed 0.6, but the spherical harmonic models of gravity (*18*) and topography (*19*) inadequately sample the southern hemisphere of the planet because of the eccentric orbit of the MESSENGER (MErcury Surface, Space ENvironment, GEochemistry, and Ranging) spacecraft. Our expectations are that at high degrees, Mercury should display a coherence broadly similar to that of the Moon, because of its heavily cratered surface. The lithosphere of Mars is heavily cratered in the southern hemisphere, but in the northern hemisphere and on the Tharsis rise, volcanic resurfacing extended well past the period of high impact flux. The extent to which the observed coherence of Mars reflects crustal structure as opposed to the quality of the data is not clear.

The free-air and Bouguer gravity anomaly maps in Fig. 1 show the distinctive character of the lunar gravity field. The free-air map shows rich short-wavelength structure and resolves virtually all craters on the Moon greater than 30 km

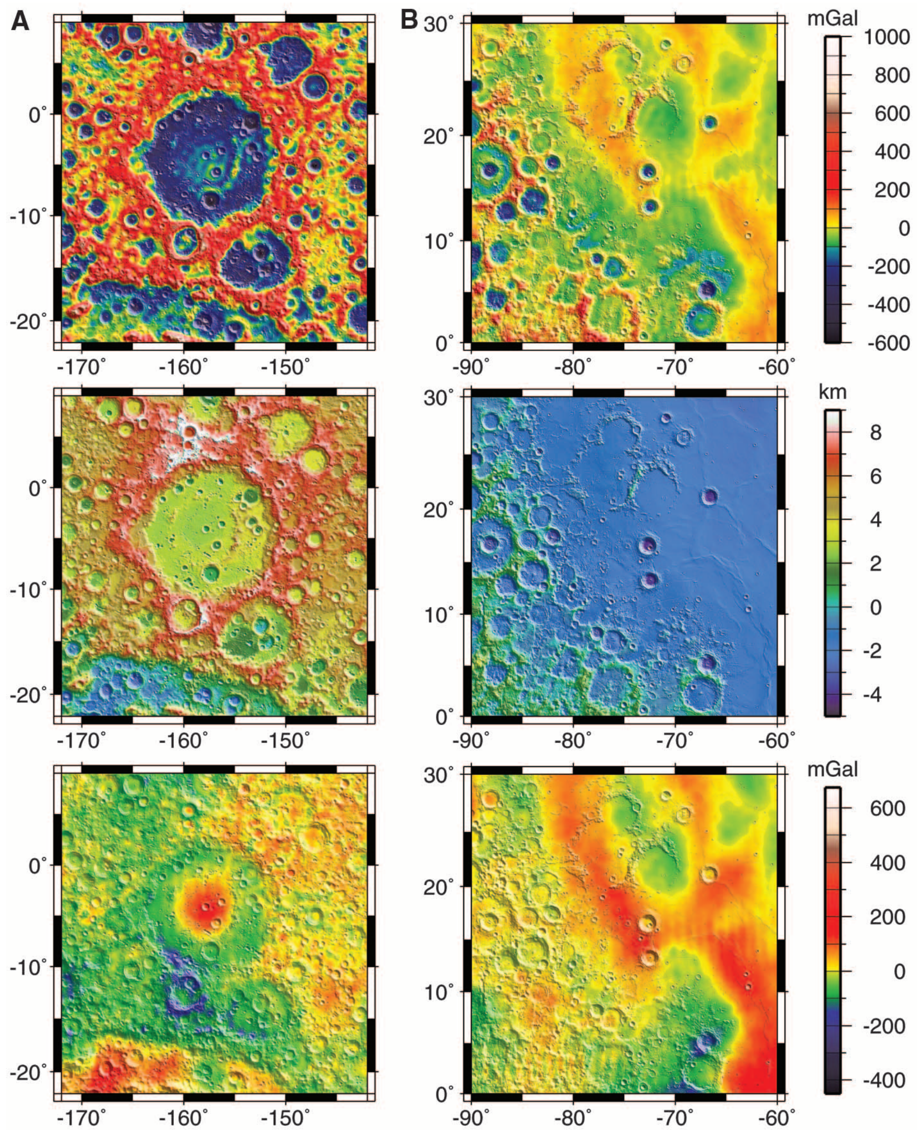

Fig. 3. (**A** and **B**) From top to bottom, Mercator projections of free-air gravity, topography, and Bouguer gravity. Frames in (A) highlight the area surrounding the Korolev impact basin, at center. Frames in (B) show the western limb of Oceanus Procellarum. Details of free-air and Bouguer gravity are the same as in Fig. 1. Topography is from a LOLA 1/64° grid.

in diameter and many less than 20 km in diameter. The highlands, because of the higher density of impact structures, show more gravitational detail at short wavelengths than the volcanic plains of the maria. In comparison with the free-air gravity, the Bouguer map is smooth at short wavelengths because the contributions to free-air gravity from impact craters derive mostly from their topography. This characteristic of lunar structure facilitates the isolation of density variations within the crust (*20*). As noted in previous studies (*5*, *21*), large impact basins are accompanied by thinning of the crust beneath the basin cavity, due to excavation and rebound associated with the impact and basin formation process (*22*). In some cases, there is a second contribution from partial fill by mare volcanic deposits after basin formation.

Regional comparisons of the free-air gravity anomaly, topography (*23*), and Bouguer gravity anomaly reveal features that inform understanding of lunar structure and evolution. For instance, Fig. 3A shows an area of the farside highlands that includes the 417-km–diameter Korolev basin as well as many complex and simple craters. The maps also illustrate the ability of GRAIL to resolve Korolev's peak ring. In contrast to previous fields, GRAIL resolves Korolev's central Bouguer high to lie entirely within the central peak ring, and the annular low to reside on the crater floor and not beneath the walls. The observed gravitational structure implies that there is a density deficit under the floor due either to less dense, possibly brecciated, surface material filling the interior of Korolev but restricted to areas outside the peak ring, or to thickened crust produced by subisostatic depression of the crust/mantle boundary.

Also evident in Fig. 3A is the spatial manifestation of the Moon's high coherence: The free-air map resembles the topography map at intermediate to short length scales. In contrast, the Bouguer map is generally smooth; removal of the gravitational attraction of topography reveals that there is much less short-wavelength structure attributable to subsurface density variations. Thinning of the crust beneath Korolev (*24*) represents the primary contribution to subsurface density variations in this area. The negative Bouguer signature of the rim of Doppler crater, just to the south of Korolev, may be indicative of brecciation and/or ejecta.

A region in the western part of Oceanus Procellarum (Fig. 3B) highlights the subsurface structure of maria and underlying crust in this region. Positive Bouguer gravity anomalies in the maria are part of a pattern in western and southern Oceanus Procellarum (Fig. 1B) that may indicate locally denser or thicker mare material. These Bouguer anomalies may help to define the boundary of either the Procellarum KREEP Terrane (*25*) or of the proposed Procellarum impact basin (*26*).

As exemplified by Fig. 3B, gravitational evidence for fully buried craters in the maria is not abundant. The gravitational signature of a buried crater should include two effects of opposite sign. A contribution from the subsurface, which for fresh craters tends to be fractured and brecciated and therefore less dense than surrounding crust, should produce a negative anomaly. In contrast, because mare material is more dense than highland crust, a greater thickness over the floor of the buried crater should contribute a positive anomaly. Figure 3C shows that two partially buried craters between 20° to 30°N and –80° to –70°E display negative anomalies that suggest that for these structures, the contribution from subsurface structure dominates. Systematic study of other mare regions will provide insight into the thickness of infill and the underlying highland structure (*27*).

Results from GRAIL's PM provide a detailed view of the structure of the lunar crust and bring quantitative geophysical description of the internal structure of the Moon into a spatial realm commensurate with the scale of surface geological features. More broadly, the observed gravitational structure increases understanding of the role of impact bombardment on the crusts of terrestrial planetary bodies.

References and Notes

1. M. T. Zuber, D. E. Smith, D. H. Lehman, M. M. Watkins, *Int. Astronaut. Congress* **12**, B4 (2012).
2. P. M. Muller, W. L. Sjogren, *Science* **161**, 680 (1968).
3. N. Namiki *et al.*, *Science* **323**, 900 (2009).
4. Materials and methods are available as supplementary materials on *Science* Online.
5. A. S. Konopliv *et al.*, *Science* **281**, 1476 (1998).
6. A. S. Konopliv, S. W. Asmar, E. Carranza, W. L. Sjogren, D.-N. Yuan, *Icarus* **150**, 1 (2001).
7. E. Mazarico, F. G. Lemoine, S.-C. Han, D. E. Smith, *J. Geophys. Res.* **115**, E05001 (2010).
8. B. D. Tapley, S. Bettadpur, J. C. Ries, P. F. Thompson, M. M. Watkins, *Science* **305**, 503 (2004).
9. R. B. Roncoli, K. K. Fujii, "Mission design overview for the Gravity Recovery and Interior Laboratory (GRAIL) mission," paper presented at the AIAA Guidance, Navigation, and Control Conference, Toronto, Ontario, Canada, 2 to 5 August 2010, AIAA 2010-9393.
10. S. J. Hatch, R. B. Roncoli, T. H. Sweetser, "GRAIL trajectory design: Lunar orbit insertion through science," paper presented at the AIAA Astrodynamics Conference, Toronto, Ontario, CA, 2 to 5 August 2010, AIAA 2010-8385.
11. S.-C. Han, E. Mazarico, D. D. Rowlands, F. G. Lemoine, S. Goossens, *Icarus* **215**, 455 (2011).
12. M. Ohtake *et al.*, *Nature* **461**, 236 (2009).
13. M. A. Wieczorek, R. J. Phillips, *J. Geophys. Res.* **105**, 20417 (2000).
14. C. K. Shearer *et al.*, *Rev. Mineral. Geochem.* **60**, 365 (2006).
15. R. J. Phillips *et al.*, *J. Geophys. Res.* **97**, 5923 (1992).
16. D. E. Smith *et al.*, *J. Geophys. Res.* **106**, 23689 (2001).
17. M. T. Zuber *et al.*, *Science* **287**, 1788 (2000).
18. D. E. Smith *et al.*, *Science* **335**, (2012).
19. M. T. Zuber *et al.*, *Science* **336**, 217 (2012).
20. J. C. Andrews-Hanna *et al.*, *Science* **339**, 675 (2013).
21. M. T. Zuber, D. E. Smith, F. G. Lemoine, G. A. Neumann, *Science* **266**, 1839 (1994).
22. H. J. Melosh, *Impact Cratering: A Geologic Process* (Oxford Univ. Press, New York, 1989).
23. D. E. Smith *et al.*, *Geophys. Res. Lett.* **37**, L18204 (2010).
24. M. A. Wieczorek *et al.*, *Science* **339**, 671 (2013).
25. B. L. Jolliff, J. J. Gillis, L. Haskin, R. L. Korotev, M. A. Wieczorek, *J. Geophys. Res.* **105**, 4197 (2000).
26. P. H. Cadogan, *Nature* **250**, 315 (1974).
27. J. W. Head III, L. Wilson, *Geochim. Cosmochim. Acta* **56**, 2155 (1992).

Acknowledgments: The GRAIL mission is supported by NASA's Discovery Program and is performed under contract to the Massachusetts Institute of Technology and the Jet Propulsion Laboratory, California Institute of Technology. We are grateful to the GRAIL spacecraft, instrument, and operations teams for outstanding support. We thank J. Andrews-Hanna, J. Head, W. Kiefer, P. McGovern, F. Nimmo, J. Soderblom, and M. Sori for helpful comments on the manuscript. The data used in this study have been submitted to the Geosciences Node of the NASA Planetary Data System.

Supplementary Materials

www.sciencemag.org/cgi/content/full/science.1231507/DC1
Supplementary Text
Figs. S1 to S5
Table S1
References (*28–43*)

15 October 2012; accepted 27 November 2012
Published online 5 December 2012;
10.1126/science.1231507

The Crust of the Moon as Seen by GRAIL

Mark A. Wieczorek,[1]* Gregory A. Neumann,[2] Francis Nimmo,[3] Walter S. Kiefer,[4] G. Jeffrey Taylor,[5] H. Jay Melosh,[6] Roger J. Phillips,[7] Sean C. Solomon,[8,9] Jeffrey C. Andrews-Hanna,[10] Sami W. Asmar,[11] Alexander S. Konopliv,[11] Frank G. Lemoine,[2] David E. Smith,[12] Michael M. Watkins,[11] James G. Williams,[11] Maria T. Zuber[12]

High-resolution gravity data obtained from the dual Gravity Recovery and Interior Laboratory (GRAIL) spacecraft show that the bulk density of the Moon's highlands crust is 2550 kilograms per cubic meter, substantially lower than generally assumed. When combined with remote sensing and sample data, this density implies an average crustal porosity of 12% to depths of at least a few kilometers. Lateral variations in crustal porosity correlate with the largest impact basins, whereas lateral variations in crustal density correlate with crustal composition. The low-bulk crustal density allows construction of a global crustal thickness model that satisfies the Apollo seismic constraints, and with an average crustal thickness between 34 and 43 kilometers, the bulk refractory element composition of the Moon is not required to be enriched with respect to that of Earth.

The nature of the lunar crust provides crucial information on the Moon's origin and subsequent evolution. Because the crust is composed largely of anorthositic materials (*1*), its average thickness is key to determining the bulk silicate composition of the Moon (*2*, *3*)